

Article

Performance Improvement for PMSM DTC System through Composite Active Vectors Modulation

Tianqing Yuan  and Dazhi Wang *

School of Information Science and Engineering, Northeastern University, Shenyang 110819, China; tqyuan@stumail.neu.edu.cn

* Correspondence: noblefuture@163.com; Tel.: +86-133-2245-2013

Received: 19 September 2018; Accepted: 18 October 2018; Published: 22 October 2018



Abstract: In this paper, a novel direct torque control (DTC) scheme based on composite active vectors modulation (CVM) is proposed for permanent magnet synchronous motor (PMSM). The precondition of the accurate compensations of torque error and flux linkage error is that the errors can be compensated fully during the entire control period. Therefore, the compensational effects of torque error and flux linkage error in different operating conditions of the PMSM are analyzed firstly, and then, the operating conditions of the PMSM are divided into three cases according to the error compensational effects. To bring the novel composite active vectors modulation strategy smoothly, the effect factors are used to represent the error compensational effects provided by the applied active vectors. The error compensational effects supplied by single active vector or synthetic voltage vector are analyzed while the PMSM is operated in three different operating conditions. The effectiveness of the proposed CVM-DTC is verified through the experimental results on a 100-W PMSM drive system.

Keywords: direct torque control (DTC); composite active vectors modulation (CVM); permanent magnet synchronous motor (PMSM); effect factors

1. Introduction

Permanent magnet synchronous motors (PMSM) have a lot of merits such as high reliability, high efficiency, simple construction, and good control performance, and thus, it has been applied in various control systems including electrical drives, industrial applications, and medical devices in recent years [1–7]. Direct torque control (DTC) and field-oriented control (FOC) are two widely applied high-performance control strategies for the PMSM. Different from the decoupled-analyzing method in FOC, torque and flux linkage are controlled directly in DTC, and therefore, the quickest dynamic response can be obtained in the PMSM driven by DTC. However, as only six active vectors can be selected to compensate the errors of flux linkage and torque in conventional DTC (CDTC), the PMSM suffers from some drawbacks, such as large torque and flux linkage ripples. To improve the steady-state performance of the PMSM, many researchers have attempted to reduce these ripples by adding the amount of the active vectors through different methods.

With more appropriate active vectors selected in each control period, a novel DTC-fed PMSM system is proposed on the basis of a three-level inverter [8,9], and thus, the ripples of torque and flux linkage in PMSM can be suppressed effectively. In References [10,11], a novel DTC strategy using a matrix converter is proposed. Four enhanced switching tables are designed for the selection of switching states, and therefore, the ripples of the PMSM can be reduced effectively. Despite the fact that multiple active vectors can be supplied by three-level inverter or matrix converter, the cost of the DTC system is inevitably increased.

In fact, torque error and flux linkage error are tiny in most cases, and therefore, these errors will be over-compensated if the selected vector is applied over the whole control period. To solve these

problems, duty ratio modulation strategy is introduced into the DTC-fed PMSM. Different duty ratio modulation methods for DTC (DDTC) are studied in References [12–16], and the ripples of torque and flux linkage can be reduced effectively without degrading the fast dynamic response in CDTC. In Reference [17], a new suboptimal control algorithm applying dynamic programming and a ramp trajectory method is proposed to DB-DTFC. In DB-DTFC, the maximum torque changes in one inverter switching period are used to determine the number of quantized stages for the minimum-time ramp trajectory method. It can be found that, the error compensational effects are considered in DB-DTFC, and therefore, torque and flux linkage command trajectories can be developed in different shapes according to the desired objectives, and fast dynamic responses can be achieved easily.

The stator flux linkage currents are decoupled in d - q axes and controlled independently in FOC, and thus, the outstanding operating performance of the PMSM can be obtained easily. The decoupled-analysis method is adopted in the novel DTC based on a space vector modulation (SVM) strategy with simple proportional-integral (PI) regulator or sliding mode observer [18–25]. With the independent control of torque and flux linkage in SVM-DTC, the amplitude and the phase of the wanted active vector can be determined accurately, and the errors of torque and flux linkage can be compensated precisely. However, the introduced PI regulator or sliding mode observer will degrade the dynamic response of the system.

To improve the operation performance of PMSM effectively, a novel DTC scheme utilizing composite active vectors modulation (CVM) strategy is presented in this paper. The compensational effects of torque error and flux linkage error in the PMSM driven by different control strategies are analyzed. Subsequently, the precondition of the accurate error compensation is obtained, and then, the precondition is adopted to determine the applied control strategy for the PMSM in different operation conditions, which is ignored in SVM-DTC and CDTC.

It should be noted that the most complicated control process is the transient-state. The large error component should be compensated fully, and the low error component should not be over-compensated; therefore, the duty ratio direct torque control strategy which, considering the active angles and the impact angles in Reference [1], can be used. The effectiveness of the proposed CVM-DTC scheme is validated through the experimental results. It should be noted that the steady-state performance and the dynamic response of the PMSM driven by CDTC, DDTC, and SVM-DTC are also studied in this paper.

The rest of this paper comprises the following sections. The principles of the conventional DTC are analyzed in Section 2. The compensational effects of torque error and flux linkage error in the SVM-DTC system are also illustrated in Section 2. The dividing process of the PMSM operation conditions and the error compensational effect supplied by different vectors in different operation conditions are described in Section 3 and the precondition of the accurate error compensations are also analyzed in Section 3. The description of experimental setup and discussions on experimental results are given in Section 4. The conclusion is analyzed in Section 5.

2. Principle of the Conventional DTC and SVM-DTC

2.1. Principle of the Conventional DTC

In the PMSM DTC system driven by a two-level voltage source inverter, eight voltage vectors can be applied to compensate the errors of torque and flux linkage, including six active vectors V_n ($n = 1, 2, 3, 4, 5, 6$) and two null vectors (V_0 and V_7). The spatial placements of the six active vectors in $\alpha\beta$ -reference frames are shown in Figure 1. The whole rotation space of stator flux linkage φ_s can be divided into six sectors through the section boundary lines l_i ($i = 1, 2, 3, 4, 5, 6$), as shown in Figure 1. The six sectors are represented with number “ N ”, and the sector vector v_s represents the active vector in every sector which the stator flux linkage φ_s is located in.

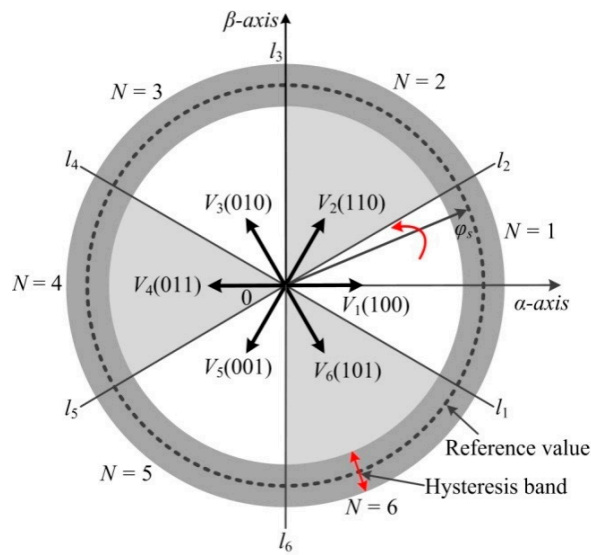


Figure 1. Active vectors in DTC system.

The torque error e_T is obtained by the comparison between the reference value T_{ref} and the real-time value T . The hysteresis comparator is used to determine the property ε_T of torque error e_T . The property ε_T value is 1 or -1 , which indicates torque T needs to be increased if the value of property ε_T is 1, while the torque needs to be decreased if the value of property ε_T is -1 . The determination methods of another parameter flux linkage φ is in the same way. The active vector selection rules in the SV-CDTC system are described in Table 1.

Table 1. Conventional switching table.

Sector number N	Torque (ε_T)	
	1	-1
Stator flux linkage (ε_F)	1	V_{N+1} V_{N-1}
	-1	V_{N+2} V_{N-2}

2.2. Compensations of Torque Error and Flux Linkage Error in SVM-DTC System

The number and the direction of the active vectors are fixed in CDTC, and therefore, the errors of torque and flux linkage are difficult to be compensated effectively, leading to large ripples. To improve the steady-state performance of the PMSM, the decoupling control strategy adopted in FOC is introduced into DTC. The PI controllers are used to obtain the amplitude of the torque vector and flux linkage vector on the basis of torque error and flux linkage error; then, the space vector modulation (SVM) is used to determine the precise vectors. The schematic diagram of SVM-DTC is shown in Figure 2.

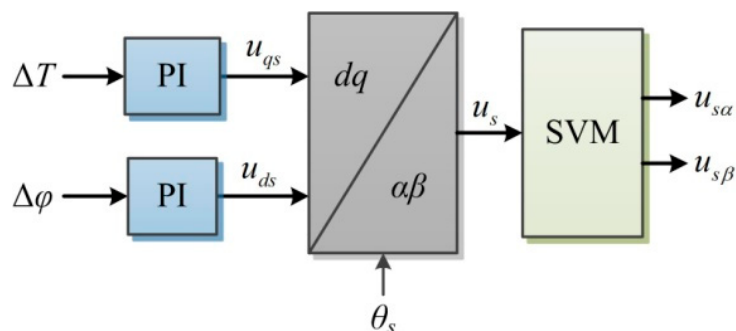


Figure 2. Schematic diagram of SVM-DTC.

Figure 2 shows the error compensations provided by a synthesis voltage vector. It can be found that torque error ΔT and flux linkage error $\Delta\varphi$ can be compensated through vectors u_{qs} and u_{ds} , respectively. Consequently, the synthesis voltage vector u_s can be obtained on the basis of the rotor position θ_s . As shown in Figure 3, the voltage vectors $u_{s\alpha}$ and $u_{s\beta}$ will be obtained through coordinate transformation based on u_s .

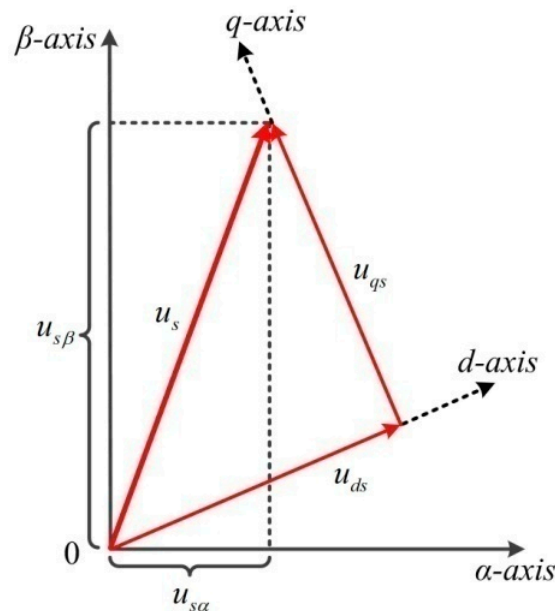


Figure 3. Synthesis voltage vectors in d - q reference frame.

From the aforementioned analyses, it can be observed that the switching table in CDTC is replaced by the PI controllers in SVM-DTC. Therefore, the active vectors used to compensate the errors of torque and flux linkage are not limited to the six basic active vectors. Additionally, the ideal steady-state performance of the PMSM can be obtained easily. Despite the fact that the precision of the wanted synthetic vector can be ensured with the using of SVM strategy in SVM-DTC, the dynamic response of the PMSM is affected inevitably.

3. Analysis of Error Compensations

The ripples of torque and flux linkage in the PMSM driven by SVM-DTC are relatively minor while the PMSM is operated in the steady-state condition. On the other hand, the dynamic performance will be affected by the complicated calculations of the synthesis voltage vector and the over-modulation process while the PMSM is operated in the dynamic response condition. This is the main reason that the fast dynamic performance of permanent magnet synchronous motor driven by SVM-DTC is degraded.

To improve the steady-state performance of PMSM, and maintain the fast dynamic response at the same time, appropriate control strategy should be selected and applied to the system according to the operation conditions, including CDTC, DDTC, and SVM-DTC. Therefore, the differences of the error compensational effects provided by the synthesis voltage vector and single active vector under different operation conditions should be analyzed firstly.

3.1. Operation Conditions

The stator flux linkage φ_s changes from φ_{s1} to φ_{s2} during one control period and the variation of the stator flux linkage φ_s is $\Delta\varphi_s$, which can be decoupled into $\Delta\varphi_{sd}$ and $\Delta\varphi_{sq}$ in the d - q axis. In this control period, the errors of torque and flux linkage are ΔT and $\Delta\varphi$, respectively. Hence, the torque

component variation of the stator flux linkage is $\Delta\varphi_{sq}$, and the amplitude component variation of the stator flux linkage is $\Delta\varphi_{sd}$, as shown in Figure 4.

The torque component variation and the amplitude component variation of the stator flux linkage can be expressed as

$$\Delta\varphi_{sq} = \frac{2L_s}{3p} \cdot \frac{1}{\varphi_f} \cdot \Delta T \tag{1}$$

$$\Delta\varphi_{sd} = \Delta\varphi \tag{2}$$

where L_s is the stator inductance, p is the number of pole pairs, and φ_f is the permanent magnet flux linkage.

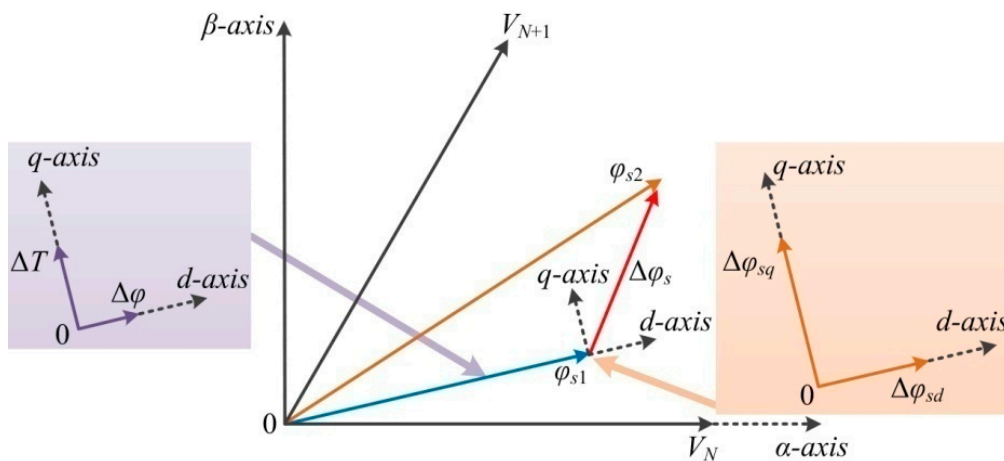


Figure 4. Analysis of error compensational effects.

The compensational effect of the stator flux linkage supplied by single active vector V_N and synthesis voltage vector u_s are $\Delta\varphi'_{s1}$ and $\Delta\varphi'_{s'}$, respectively, as shown in Figure 5.

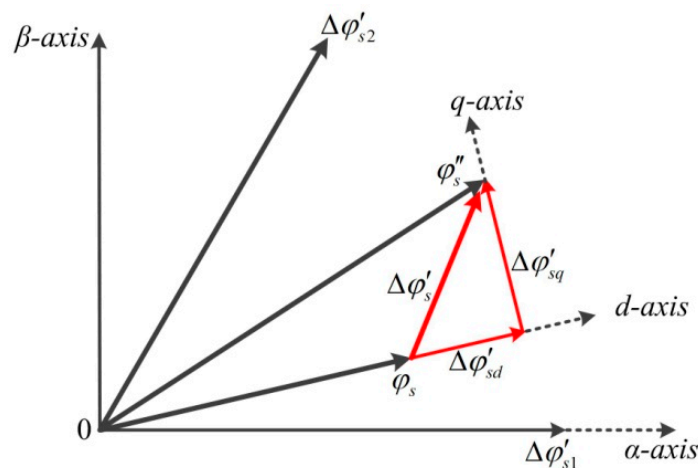


Figure 5. Analysis of error compensational effects.

The torque component compensation of the stator flux linkage supplied by synthesis voltage vector u_s is $\Delta\varphi'_{sq'}$, and the amplitude component compensation of the stator flux linkage provided by synthesis voltage vector u_s is $\Delta\varphi'_{sd'}$. It is obvious that the parameters of $\Delta\varphi'_{s'}$, $\Delta\varphi'_{sq'}$, and $\Delta\varphi'_{sd'}$ are fixed during each control period in the system. While the torque error ΔT and the flux linkage error $\Delta\varphi$ will vary with the variation of the stator flux linkage location in different control period. Therefore, the real values of $\Delta\varphi_{sq}$ and $\Delta\varphi_{sd}$ are also different.

The relationships between the real error compensations of the stator flux linkage and the errors can be described in the following way.

First item, the actual compensations are greater than the errors:

$$\begin{pmatrix} \Delta\varphi'_{sd} > \Delta\varphi_{sd} \\ \Delta\varphi'_{sq} > \Delta\varphi_{sq} \end{pmatrix} \quad (3)$$

Second item, the actual compensations are less than the errors:

$$\begin{pmatrix} \Delta\varphi'_{sd} < \Delta\varphi_{sd} \\ \Delta\varphi'_{sq} < \Delta\varphi_{sq} \end{pmatrix} \quad (4)$$

Third item, the actual compensation of the amplitude component is less than the error while the actual compensation of torque component is greater than the error:

$$\begin{pmatrix} \Delta\varphi'_{sd} < \Delta\varphi_{sd} \\ \Delta\varphi'_{sq} > \Delta\varphi_{sq} \end{pmatrix} \quad (5)$$

Fourth item, the actual compensation of the amplitude component is greater than the error while the actual compensation of torque component is less than the error:

$$\begin{pmatrix} \Delta\varphi'_{sd} > \Delta\varphi_{sd} \\ \Delta\varphi'_{sq} < \Delta\varphi_{sq} \end{pmatrix} \quad (6)$$

The operation conditions of the PMSM can be divided into three items in accordance with the errors and the actual compensations, as shown in Table 2.

Table 2. Operation conditions

Operation Conditions	Reference Equation
Steady-state	(3)
Transient-state	(5) and (6)
Dynamic-state	(4)

3.2. Error Compensation Analysis in Steady-State Case

The values of torque error ΔT and flux linkage error $\Delta\varphi_s$ are relatively low in steady-state case [6]. The angle between the stator flux linkage φ_s and the active vector V_N is θ_1 , as shown in Figure 6. It is also shown in Figure 6 that both the compensations of ΔT and $\Delta\varphi_s$ are bigger than the errors. Consequently, the errors will be over-compensated if the active vector or the synthesized voltage vector is applied during the entire control period.

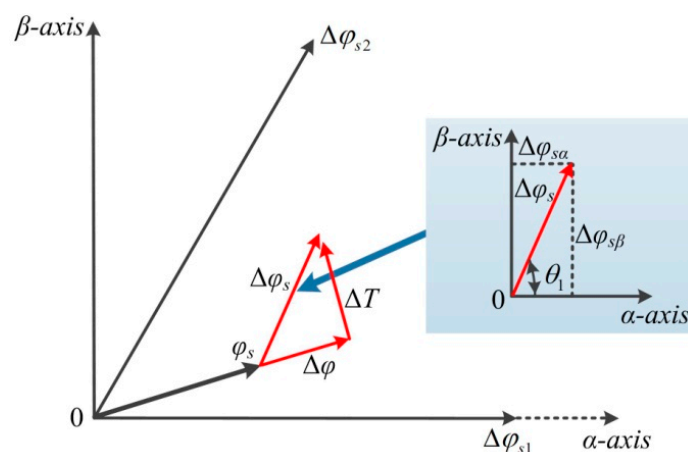


Figure 6. Analysis of error compensational effects in steady-state.

In DDTC-fed PMSM, the applied time of the active vector is modulated by duty ratio modulation strategy. As a result, the over-compensation of the errors can be avoided; nevertheless, the fixed active vectors limit the compensational effects.

In the PMSM driven by SVM-DTC, the adjacent active vectors V_N and V_{N+1} are selected as the benchmark vectors to obtain the synthesized voltage vector u_s . Furthermore, the applied time of V_N and V_{N+1} are T_1 and T_2 , respectively. The error compensations can be evaluated by

$$\Delta\varphi_{s1} = V_N \cdot T_1 \tag{7}$$

$$\Delta\varphi_{s2} = V_{N+1} \cdot T_2 \tag{8}$$

The modulation process of the active vectors can be expressed as

$$\Delta\varphi_{s1} + \Delta\varphi_{s2} \cdot \cos \frac{\pi}{3} = \Delta\varphi_{s\alpha} = \Delta\varphi_s \cdot \cos \theta_1 \tag{9}$$

$$\Delta\varphi_{s2} \cdot \sin \frac{\pi}{3} = \Delta\varphi_{s\beta} = \Delta\varphi_s \cdot \sin \theta_1 \tag{10}$$

$$T_1 + T_2 + T_0 = T_s \tag{11}$$

where T_0 is the zero voltage vector applied time.

From the aforementioned analyses, it can be found that the errors of torque and flux linkage can be compensated accurately through SVM strategy while the PMSM is operated in steady-state.

3.3. Error Compensation Analysis in Dynamic-State Case

The errors of torque or flux linkage may become greater in the dynamic-state while the speed or the torque changes. As shown in Figure 7, the stator flux linkage error is $\Delta\varphi_s$; the angle between the stator flux linkage error $\Delta\varphi_s$ and the active vector V_N is θ_2 . It can be found that the torque error and the flux linkage error are greater than the error compensations.

It can be found that the torque error ΔT and the flux linkage error $\Delta\varphi$ cannot be compensated fully by any single active vector or the synthesized voltage vector in the next control period. The differences of the error compensation effect supplied by the single active vector or the synthesized voltage vector are described in following parts.

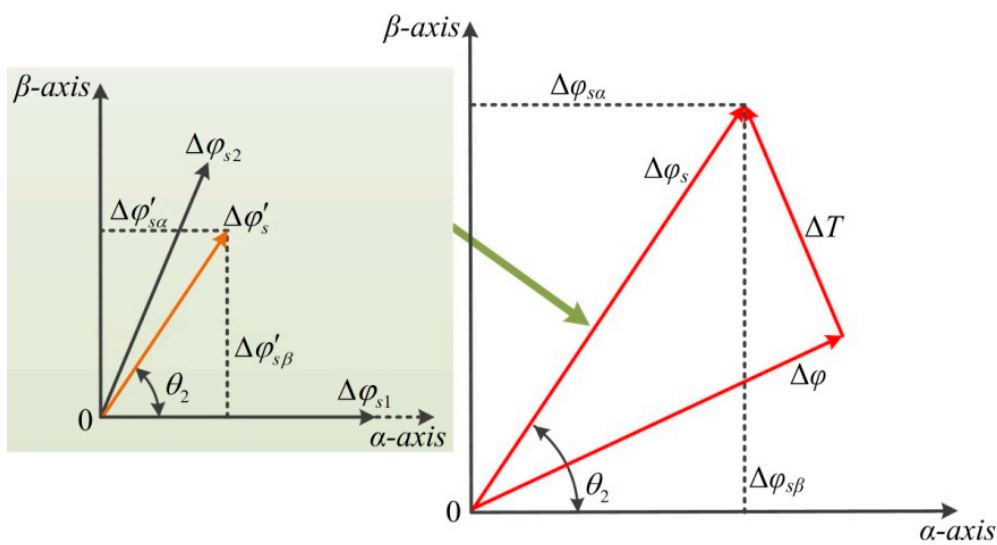


Figure 7. Analysis of error compensational effects in dynamic-state.

3.3.1. Synthetic Voltage Vector

The adjacent active vectors V_N and V_{N+1} are selected as the benchmark vectors. The applied time of V_N and V_{N+1} are T_1 and T_2 , respectively. Therefore, the error compensations can be calculated as

$$\Delta\varphi'_{s1} = V_N \cdot T_1 \tag{12}$$

$$\Delta\varphi'_{s2} = V_{N+1} \cdot T_2 \tag{13}$$

$$\Delta\varphi'_{s1} + \Delta\varphi'_{s2} \cdot \cos \frac{\pi}{3} = \Delta\varphi_{s\alpha} = \Delta\varphi_s \cdot \cos \theta_2 \tag{14}$$

$$\Delta\varphi'_{s2} \cdot \sin \frac{\pi}{3} = \Delta\varphi_{s\beta} = \Delta\varphi_s \cdot \sin \theta_2 \tag{15}$$

Since the actual compensations are smaller than the errors, therefore

$$T_1 + T_2 > T_s \tag{16}$$

The applied time of the applied active vectors can be over-modulated as

$$T'_1 = \frac{T_1}{T_1 + T_2} \cdot T_s \tag{17}$$

$$T'_2 = \frac{T_2}{T_1 + T_2} \cdot T_s \tag{18}$$

The applied time of the applied active vectors can be rewritten as

$$T_1 = k_1 \cdot T_s \tag{19}$$

$$T_2 = k_2 \cdot T_s \tag{20}$$

where k_1 and k_2 are the duty ratio values of applied time of V_N and V_{N+1} , respectively.

Therefore, the actual compensation of the stator flux linkage in one control period is

$$\Delta\varphi'_{s\alpha} = V_N \cdot \frac{k_1}{k_1 + k_2} \cdot T_s + V_{N+1} \cdot \cos \frac{\pi}{3} \cdot \frac{k_2}{k_1 + k_2} \cdot T_s \tag{21}$$

$$\Delta\varphi'_{s\beta} = V_{N+1} \cdot \sin \frac{\pi}{3} \cdot \frac{k_2}{k_1 + k_2} \cdot T_s \tag{22}$$

which can be simplified as

$$\begin{cases} \Delta\varphi'_{s\alpha} = V_N \cdot T_s \cdot \left(\frac{k_1}{k_1+k_2} + \frac{1}{2} \cdot \frac{k_2}{k_1+k_2} \right) \\ \Delta\varphi'_{s\beta} = V_N \cdot T_s \cdot \frac{\sqrt{3}}{2} \cdot \frac{k_2}{k_1+k_2} \end{cases} \tag{23}$$

Therefore, the compensation of the stator flux linkage supplied by synthesized voltage vector u_s can be given as

$$|\Delta\varphi'_s| = \sqrt{(\Delta\varphi'_{s\alpha})^2 + (\Delta\varphi'_{s\beta})^2} = V_N \cdot T_s \cdot \sqrt{\frac{k_1^2 + k_1k_2 + k_2^2}{(k_1 + k_2)^2}} < V_N \cdot T_s \tag{24}$$

3.3.2. Single Active Vector

The compensations of the stator flux linkage supplied by adjacent vectors V_N and V_{N+1} during the whole control period are

$$\Delta\varphi''_{s1} = V_N \cdot T_s \tag{25}$$

$$\Delta\varphi''_{s2} = V_{N+1} \cdot T_s \tag{26}$$

Therefore, the compensations of the stator flux linkage provided by the single active vector can be expressed as

$$\Delta\varphi''_s = \Delta\varphi''_{s1} = \Delta\varphi''_{s2} = V_N \cdot T_s \tag{27}$$

The comparison result of the stator flux linkage compensations supplied by the different vectors can be described as

$$\Delta\varphi'_s < \Delta\varphi''_s \tag{28}$$

From the aforementioned analyses, it can be observed that the compensational effects of the stator flux linkage supplied by the synthesized voltage vector is weaker than the single active vector. Therefore, the SVM strategy is not required to compensate the errors of torque and flux linkage while the PMSM is operated in the dynamic state. To simplify the calculations of the system, the appropriate active vector can be selected from a conventional switching table and be used in the system over the entire control period.

In short, CDTC strategy should be used to reduce the ripples of torque and flux linkage in the PMSM when the PMSM is operated in a dynamic state. Hence, the delayed dynamic response caused by the PI controller can be eliminated, and the ripples' depressing effects of the PMSM driven by CDTC are the same as that driven by SVM-DTC.

3.4. Error Compensation Analysis in Transient-State Case

The operation condition of the PMSM may deviate the steady-state due to external disturbance. Therefore, the PMSM may operate in a transient-state if one parameter of torque error and flux linkage error is large while another parameter is relatively low.

The torque error ΔT is high and the flux linkage error $\Delta\varphi$ is relatively low as shown in Figure 8. The variation of the stator flux linkage is $\Delta\varphi_s$.

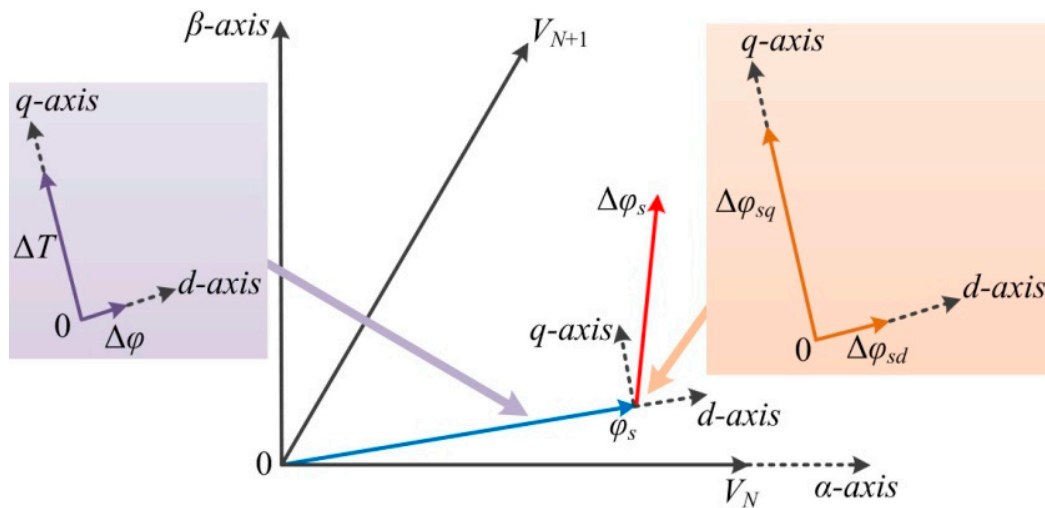


Figure 8. Analysis of error compensational effects in transient-state.

The differences of the error compensation effect supplied by single active vector or synthesized voltage vector are described in the following section.

3.4.1. Synthetic Voltage Vector

Figure 9 shows the error compensational effects provided by different active vectors.

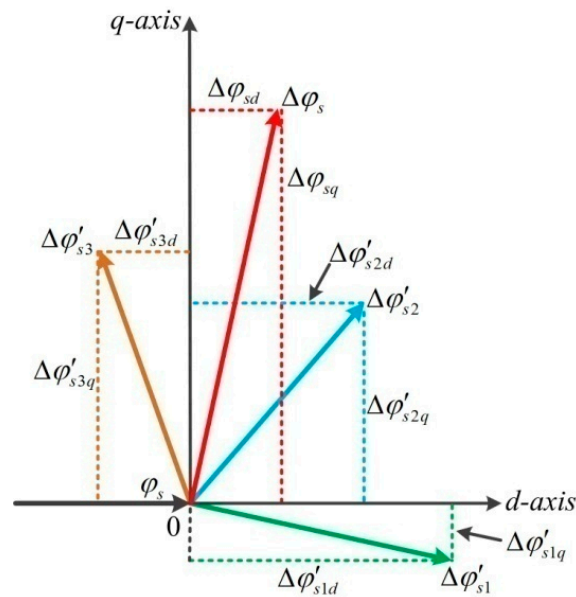


Figure 9. Analysis of error compensational effects provided by different active vectors.

As shown in Figure 9, the adjacent active vectors V_{N+1} and V_{N+2} are selected as the benchmark vectors. The applied time of V_{N+1} and V_{N+2} are T_1 and T_2 , respectively. Therefore, the error compensations can be evaluated by

$$\Delta\phi'_{s2q} \cdot T_1 + \Delta\phi'_{s3q} \cdot T_2 = \Delta\phi_{sq} \cdot T_s \tag{29}$$

$$\Delta\phi'_{s2d} \cdot T_1 - \Delta\phi'_{s3d} \cdot T_2 = \Delta\phi_{sq} \cdot T_s \approx 0 \tag{30}$$

3.4.2. Single Active Vector V_n

The stator flux linkage error $\Delta\phi_s$ is located in the middle of error compensations $\Delta\phi'_{s2}$ and $\Delta\phi'_{s3}$, as shown in Figure 9. To compensate the error $\Delta\phi_{sq}$ effectively and avoid the over-compensation of the error $\Delta\phi_{sd}$ at the same time, the adjacent vectors V_{N+1} and V_{N+2} can be selected and applied to half of the control period.

From the above analysis, it can be found that the torque error can be compensated fully supplied by a single active vector while the PMSM is operated in the transient-state; however, the flux linkage error cannot be compensated fully. Despite the fact that the torque error and the flux linkage error can be compensated fully by synthetic voltage vector, the calculations of the system are inevitably increased. It should be noted that the novel DDTC strategy based on the active angle in Reference [1] has solved the problem while one parameter is large and another parameter is relatively small. Therefore, the DDTC strategy can be used to improve the performance of the system while the PMSM is operated in a transient-state.

3.5. Novel Composite Active Vectors Modulation Strategy

To improve the operation performance of the PMSM effectively, a novel composite active vectors modulation DTC (CVM-DTC) strategy considering the precondition of the accurate errors compensations is presented in this section. The schematic diagram of the presented CVM-DTC system is shown in Figure 10. The parameters in CVM-DTC are defined by:

- u_{abc} : Stator voltage;
- i_{abc} : Stator currents;
- U_{DC} : DC bus voltage;
- n : Actual rotor speed;

n_{ref} : Reference rotor speed;
 σ : Rotor position;
 T_{ref} : Reference torque;
 φ_{ref} : Reference flux linkage;
 ΔT^* : *Reference torque compensation;
 $\Delta\varphi^*$: *Reference flux linkage compensation;
 V_n : Single active vector;
 d : Duty ratio value of applied time;
 u_s : Synthetic voltage vector.

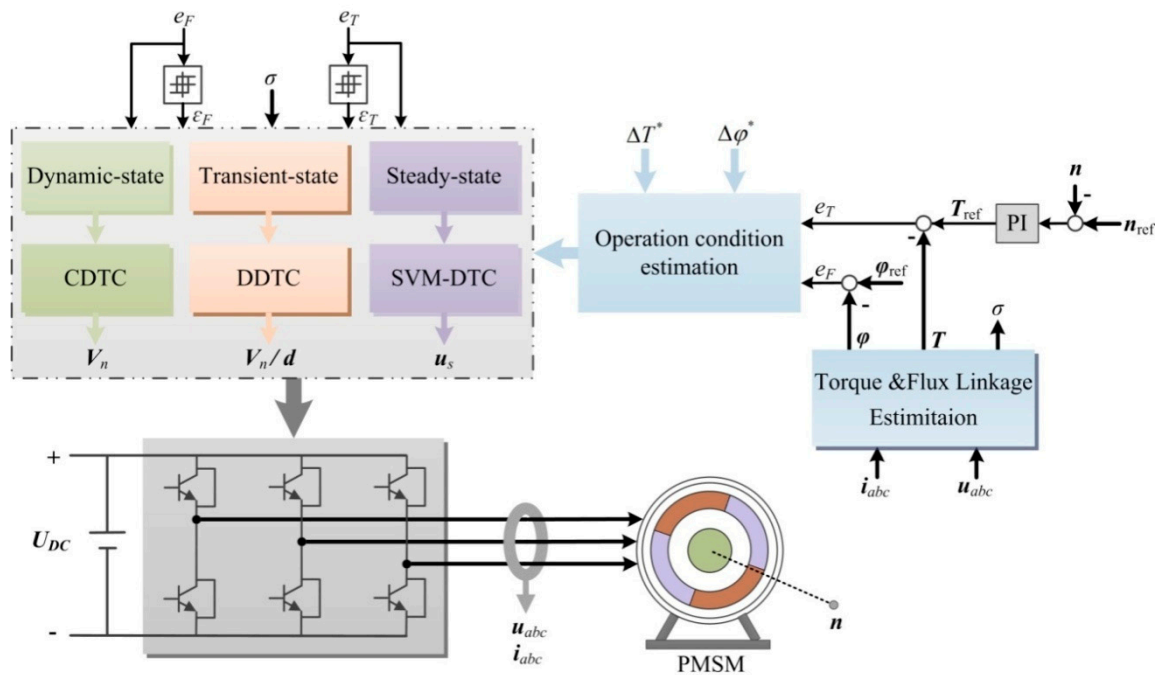


Figure 10. Schematic diagram of the CVM-DTC for PMSM.

In order to maintain the fast dynamic response in CDTC and obtain the minimum ripples of the system, the applied control strategy should adjust according to the operation conditions of the PMSM.

The precondition of the accurate compensations of torque error and flux linkage error is that the torque error and the flux linkage error can be compensated and fully supplied by the applied active vector in the whole control period. However, this precondition is ignored in the SVM-DTC system. Therefore, the torque error and the flux linkage error will be analyzed through decoupled calculations through PI controllers, while the compensational effects of the stator flux linkage in SVM-DTC and CDTC when the PMSM is operated in non-steady-state are nearly the same. As a result, the error compensational effects are not satisfied and the dynamic response will be affected without considering the operation conditions of the PMSM.

3.6. Determining of the Operation Condition through Effect Factors

The relationship between the active vector V_n and the stator flux linkage variation $\Delta\varphi_s$ in each control period is

$$\Delta\varphi_s = V_n \cdot T_s \tag{31}$$

During the whole control period, the max compensations of $\Delta\varphi_{sq}$ and $\Delta\varphi_{sd}$ can be expressed as

$$\Delta\varphi_{sq-max} = \Delta\varphi_s = V_n \cdot T_s \tag{32}$$

$$\Delta\varphi_{sd-\max} = \Delta\varphi_s = V_n \cdot T_s \quad (33)$$

The max compensation of the torque is

$$\Delta T_{\max} = \frac{3p}{2L_s} \cdot \varphi_f \cdot V_n \cdot T_s \quad (34)$$

And the max compensation of the flux linkage is

$$\Delta\varphi_{d\max} = V_n \cdot T_s \quad (35)$$

Defining the reference values of torque variation and flux linkage variation are ΔT^* and $\Delta\varphi^*$, respectively, which can be expressed as

$$\Delta T^* = \Delta T_{\max} = \frac{3p}{2L_s} \cdot \varphi_f \cdot V_n \cdot T_s \quad (36)$$

$$\Delta\varphi^* = \Delta\varphi_{d\max} = V_n \cdot T_s \quad (37)$$

The effect factors of torque and flux linkage are k_T and k_φ , respectively, which can be given as

$$k_T = \frac{\Delta T}{\Delta T^*} \quad (38)$$

$$k_\varphi = \frac{\Delta\varphi}{\Delta\varphi^*} \quad (39)$$

The introduced effect factors can be obtained through the errors and the reference values of the variation in any control period. The operation conditions of the PMSM can be classified into three cases: steady-state, transient-state, and dynamic-state. The relationships between the effect factors and the operation conditions are shown in Table 3.

Table 3. Effect factors for different operation conditions.

Effect Factors		Operation Conditions
k_T	k_φ	
$(-\infty, -1)$	$(-\infty, -1)$	Dynamic-state
	$(-1, 1)$	Transient-state
	$(1, +\infty)$	Dynamic-state
$(-1, 1)$	$(-\infty, -1)$	Transient-state
	$(-1, 1)$	Steady-state
	$(1, +\infty)$	Transient-state
$(1, +\infty)$	$(-\infty, -1)$	Dynamic-state
	$(-1, 1)$	Transient-state
	$(1, +\infty)$	Dynamic-state

4. Experimental Analysis

4.1. Experimental System Setup

Experimental studies are carried out on a 100-W PMSM drive system to validate the feasibility and effectiveness of the proposed CVM-DTC strategy. The experimental hardware setup is illustrated in Figure 11. The parameters of the PMSM are given as follows: $R_s = 0.76 \Omega$; $L_s = 0.00182 \text{ H}$; the number of pole pairs $p = 4$. The DC voltage is 36 V. This study compares the steady-state and the dynamic response performance of CDTC, DDTC, SVM-DTC, and CVM-DTC. The experiments are implemented in a TMS320F28335 DSP control system with a sampling period of 100 μs .

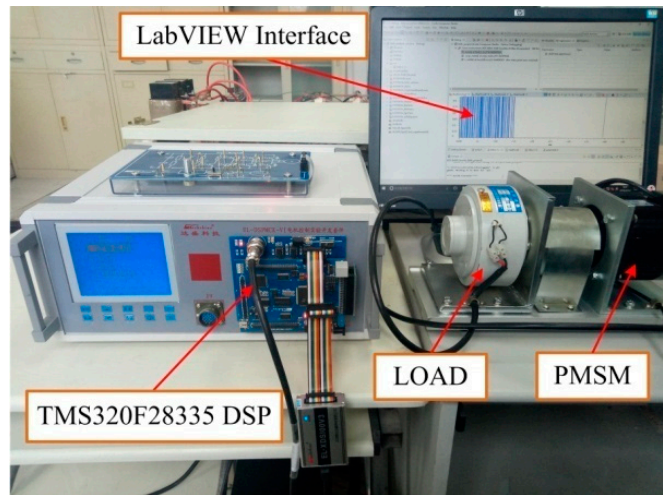


Figure 11. Experimental setup of control system.

4.2. Steady-State Performance

The steady-state performances of CDTC, DDTC, SVM-DTC, and CVM-DTC are compared under the same operating conditions. The PMSM is operated at 500 rpm and the reference values of torque and flux linkage are 0.8 N·m and 0.3 Wb, respectively. The torque and flux linkage waveforms of the PMSM are driven by different control strategies as shown in Figure 12.

From these experimental results, it can be found that the torque ripples of CDTC, SV-DDTC, SVM-DTC, and CVM-DTC are 0.56, 0.4, 0.32, and 0.34 N·m, respectively, and the flux linkage ripples of the four control system are 0.08, 0.06, 0.04, and 0.038 Wb, respectively. Therefore, compared with CDTC, DDTC and SVM-DTC can reduce the torque ripple by at least 28% and 42%, respectively, and reduce the flux linkage ripple at least 25% and 50%, respectively. While the steady-state performances of the PMSM driven by CVM-DTC in the setting operation conditions are nearly the same as SVM-DTC. The experimental results show that the errors of torque and flux should be compensated through SVM-DTC strategy, which indicates that the applied control strategy in CVM-DTC in the steady-state condition is appropriate.

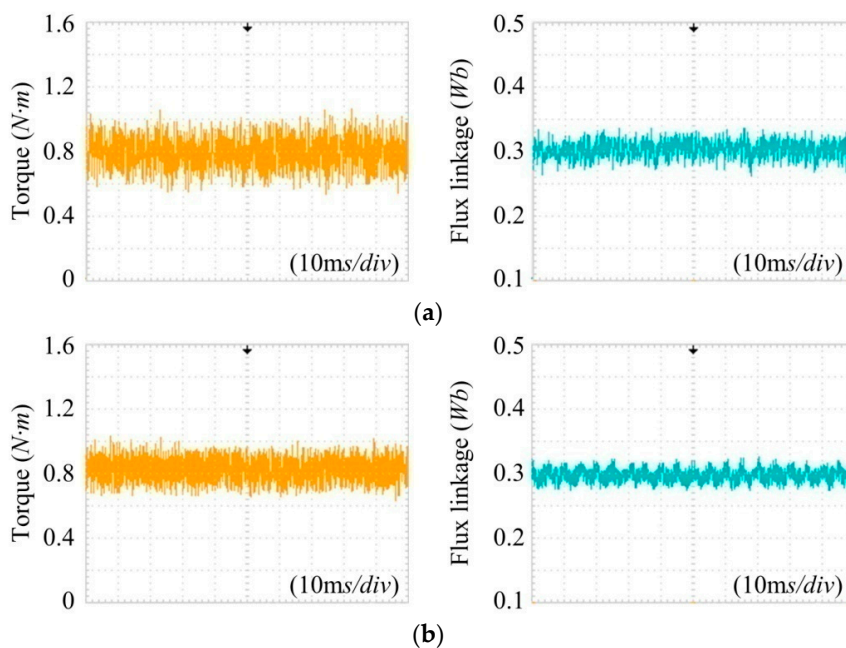


Figure 12. Cont.

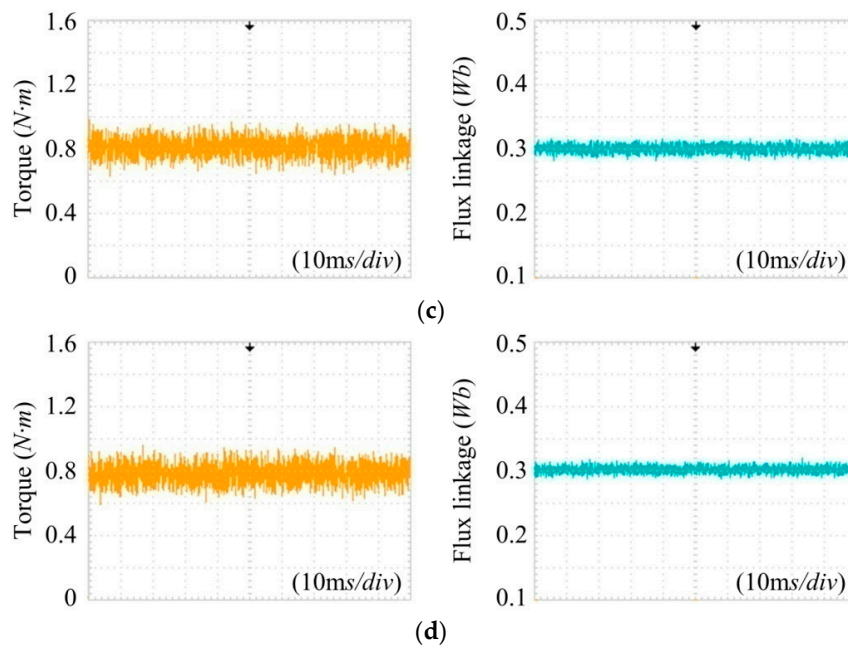


Figure 12. Experimental torque and flux linkage of the PMSM when using: (a) CDTC; (b) DDTC; (c) SVM-DTC; (d) CVM-DTC.

4.3. Dynamic Performance

To validate the fast dynamic response of the proposed novel CVM-DTC, the speed responses of the PMSM driven by the four control strategies are tested when the torque is set as 0.5 N·m. In these tests, a step change from 200 to 400 rpm is applied on the speed reference, as shown in Figure 13.

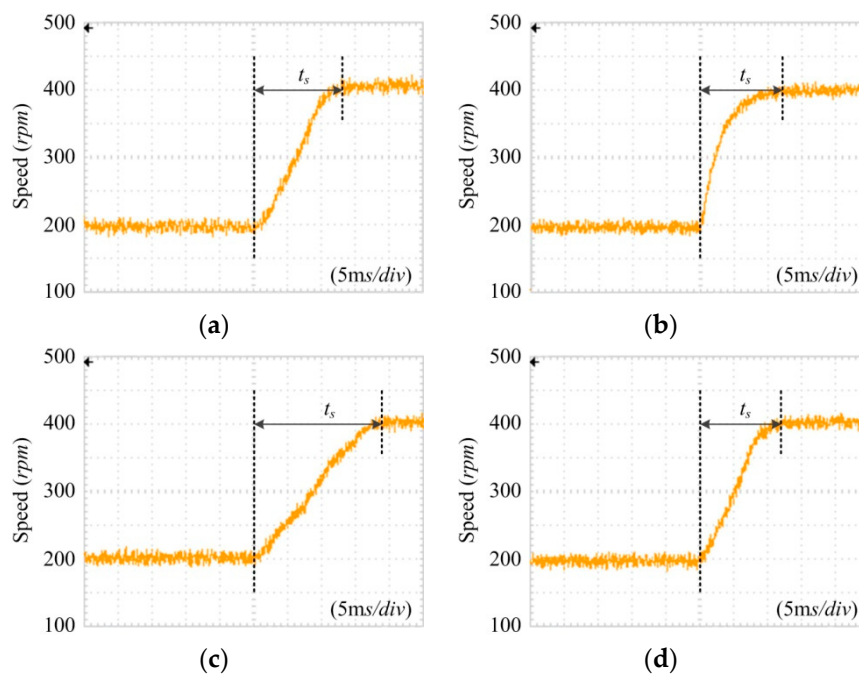


Figure 13. The speed trajectory from 200 rpm to 400 rpm when using: (a) CDTC; (b) DDTC; (c) SVM-DTC; (d) CVM-DTC.

It can be seen that the ripple of the rotor speed is 35 rpm when using CDTC, while the speed ripples of the PMSM can be reduced to 30, 25, and 24 rpm with the use of DDTC, SVM-DTC, and CVM-DTC.

Moreover, the settling times of the rotor speed using the four different control strategies are 0.013, 0.012, 0.019, and 0.012 s.

Therefore, the main advantage of CDTC, i.e., the fast dynamic response, is maintained in CVM-DTC. The experimental results show that dynamic response has a higher priority than ripples in dynamic-state condition, hence, DDTC or SVM-DTC should be abandoned. In short, the applied control strategy in CVM-DTC in the dynamic-state condition is appropriate.

5. Conclusions

The precondition of the accurate compensations of torque error and flux linkage error is considered in the proposed novel CVM-DTC scheme in this paper, which is ignored in CDTC and SVM-DTC. Therefore, the compensational effects of torque error and flux linkage error provided by the single active vector or synthetic voltage vector in different operation conditions are analyzed firstly, and then, the operating conditions of the PMSM are divided into three cases according to the compensational effects (effect factors). To improve the performance of the PMSM effectively, the applied control strategy for the PMSM in different sampling periods will vary on the basis of the introduced effect factors.

Experimental results clearly indicate that the novel CVM-DTC scheme exhibits excellent control of torque and flux linkage with lower steady-state ripples when compared to CDTC and DDTC, and faster transient response performances when compared to SVM-DTC.

Author Contributions: This paper was a collaborative effort between the authors. T.Y. and D.W. proposed the original idea; T.Y. wrote the full manuscript and carried out the experiments.

Funding: This research received no external funding.

Acknowledgments: This work was supported in part by National Natural Science Foundation of China under Grant 61,433,004 and 51467017, and in part by National Key Research and Development Program of China under Grant 2017YFB1300900.

Conflicts of Interest: The authors declare no conflict of interest.

References

1. Cheema, M.A.M.; Fletcher, J.E.; Xiao, D.; Rahman, M.F. A direct thrust control scheme for linear permanent magnet synchronous motor based on online duty ratio control. *IEEE Trans. Power Electron.* **2016**, *31*, 4416–4428. [[CrossRef](#)]
2. Abosh, A.; Zhu, Z.Q.; Ren, Y. Reduction of torque and flux ripples in space vector modulation-based direct torque control of asymmetric permanent magnet synchronous machine. *IEEE Trans. Power Electron.* **2017**, *32*, 2976–2986. [[CrossRef](#)]
3. Zhou, Y.Z.; Chen, G.T. Predictive DTC Strategy with fault-tolerant function for six-phase and three-phase PMSM series-connected drive system. *IEEE Trans. Ind. Electron.* **2018**, *65*, 9101–9112. [[CrossRef](#)]
4. Shinohara, A.; Inoue, Y.; Morimoto, S.; Sanada, M. Direct calculation method of reference flux linkage for maximum torque per ampere control in DTC-based IPMSM drives. *IEEE Trans. Power Electron.* **2016**, *32*, 2114–2122. [[CrossRef](#)]
5. Alsofyani, I.M.; Idris, N.R.N.; Lee, K.B. Dynamic hysteresis torque band for improving the performance of lookup-table-based DTC of induction machines. *IEEE Trans. Power Electron.* **2018**, *33*, 7959–7970. [[CrossRef](#)]
6. Yuan, T.Q.; Wang, D.Z.; Li, Y.L. Duty ratio modulation strategy to minimize torque and flux linkage ripples in IPMSM DTC system. *IEEE Access.* **2017**, *5*, 14323–14332. [[CrossRef](#)]
7. Putri, A.K.; Rick, S.; Franck, D.; Hameyer, K. Application of sinusoidal field pole in a permanent-magnet synchronous machine to improve the NVH behavior considering the MTPA and MTPV operation area. *IEEE Trans. Ind. Appl.* **2016**, *52*, 2280–2288. [[CrossRef](#)]
8. Tatte, Y.N.; Aware, M.V.; Pandit, J.K.; Nemade, R. Performance improvement of three-level five-phase inverter-fed DTC-controlled five-phase induction motor during low-speed operation. *IEEE Trans. Ind. Appl.* **2018**, *54*, 2349–2357. [[CrossRef](#)]
9. Payami, S.; Behera, R.K.; Iqbal, A. DTC of three-level NPC inverter fed five-phase induction motor drive with novel neutral point voltage balancing scheme. *IEEE Trans. Power Electron.* **2018**, *33*, 1487–1500. [[CrossRef](#)]

10. Xia, C.; Zhao, J.; Yan, Y.; Shi, T. A novel direct torque and flux control method of matrix converter-fed PMSM drives. *IEEE Trans. Power Electron.* **2014**, *29*, 5417–5430. [[CrossRef](#)]
11. Yan, Y.; Zhao, J.; Xia, C.; Shi, T. Direct torque control of matrix converter-fed permanent magnet synchronous motor drives based on master and slave vectors. *IET Power Electron.* **2015**, *8*, 288–296. [[CrossRef](#)]
12. Mohan, D.; Zhang, X.; Foo, G.H.B. A simple duty cycle control strategy to reduce torque ripples and improve low-speed performance of a three-level inverter fed DTC IPMSM drive. *IEEE Trans. Ind. Electron.* **2017**, *64*, 2709–2721. [[CrossRef](#)]
13. Niu, F.; Wang, B.; Babel, A.S.; Li, K.; Strangas, E.G. Comparative evaluation of direct torque control strategies for permanent magnet synchronous machines. *IEEE Trans. Power Electron.* **2016**, *31*, 1408–1424. [[CrossRef](#)]
14. Zhang, Y.; Zhu, J.; Xu, W.; Guo, Y. A simple method to reduce torque ripple in direct torque-controlled permanent-magnet synchronous motor by using vectors with variable amplitude and angle. *IEEE Trans. Ind. Electron.* **2011**, *58*, 2848–2859. [[CrossRef](#)]
15. Ren, Y.; Zhu, Z.Q.; Liu, J. Direct torque control of permanent-magnet synchronous machine drives with a simple duty ratio regulator. *IEEE Trans. Ind. Electron.* **2014**, *61*, 5249–5258. [[CrossRef](#)]
16. Niu, F.; Li, K.; Wang, Y. Direct torque control for permanent magnet synchronous machines based on duty ratio modulation. *IEEE Trans. Ind. Electron.* **2015**, *62*, 6160–6170. [[CrossRef](#)]
17. Lee, J.S.; Lorenz, R.D. Deadbeat direct torque and flux control of IPMSM drives using a minimum time ramp trajectory method at voltage and current limits. *IEEE Trans. Ind. Appl.* **2014**, *50*, 3795–3804. [[CrossRef](#)]
18. Mohan, D.; Zhang, X.; Foo, G. Generalized DTC strategy for multilevel inverter fed IPMSMs with constant inverter switching frequency and reduced torque ripples. *IEEE Trans. Energy Convers.* **2017**, *32*, 1031–1041. [[CrossRef](#)]
19. Zhang, Z.; Zhao, Y.; Qiao, W.; Qu, L. A space-vector-modulated sensorless direct-torque control for direct-drive PMSG wind turbines. *IEEE Trans. Ind. Appl.* **2014**, *50*, 2331–2341. [[CrossRef](#)]
20. Zhang, X.; Foo, G.H. Over-modulation of constant switching frequency based DTC for reluctance synchronous motors incorporating field-weakening operation. *IEEE Trans. Ind. Electron.* **2019**, *66*, 37–47. [[CrossRef](#)]
21. Berzoy, A.; Rengifo, J.; Mohammed, O. Fuzzy predictive DTC of induction machines with reduced torque ripple and high performance operation. *IEEE Trans. Power Electron.* **2018**, *33*, 2580–2587. [[CrossRef](#)]
22. Do, T.D.; Choi, H.H.; Jung, J.W. Nonlinear Optimal DTC Design and Stability Analysis for Interior Permanent Magnet Synchronous Motor Drives. *IEEE/ASME Trans. Mechatron* **2016**, *20*.
23. Choi, Y.-S.; Choi, H.H.; Jung, J.W. Feedback linearization direct torque control with reduced torque and flux ripples for IPMSM drives. *IEEE Trans. Power Electron.* **2016**, *31*, 3728–3737. [[CrossRef](#)]
24. Zhang, Z.; Wei, C.; Qiao, W.; Qu, L. Adaptive saturation controller-based direct torque control for permanent-magnet synchronous machines. *IEEE Trans. Power Electron.* **2016**, *31*, 7112–7122. [[CrossRef](#)]
25. Liang, D.L.; Li, J.; Qu, R.H.; Kong, W.B. Adaptive second-order sliding-mode observer for PMSM sensorless control considering VSI nonlinearity. *IEEE Trans. Power Electron.* **2018**, *33*, 8994–9004. [[CrossRef](#)]

